Noninvasive imaging of islet grafts using positron-emission tomography

Yuxin Lu*, Hoa Dang*, Blake Middleton*, Zesong Zhang*, Lorraine Washburn*, David B. Stout*, Martha Campbell-Thompson†, Mark A. Atkinson†, Michael Phelps*‡, Sanjiv Sam Gambhir*§, Jide Tian*, and Daniel L. Kaufman*‡

*Department of Molecular and Medical Pharmacology, David Geffen School of Medicine, University of California, Los Angeles, CA 90095-1735; †Department of Pathology, University of Florida, Gainesville, FL 32611; and §Department of Radiology, Bio-X Program, and Molecular Imaging Program, Stanford University, Stanford, CA 94305

Contributed by Michael Phelps, May 12, 2006

Islet transplantation offers a potential therapy to restore glucose homeostasis in type 1 diabetes patients. However, islet transplantation is not routinely successful because most islet recipients gradually lose graft function. Furthermore, serological markers of islet function are insensitive to islet loss until the latter stages of islet graft rejection. A noninvasive method of monitoring islet grafts would aid in the assessment of islet graft survival and the evaluation of interventions designed to prolong graft survival. Here, we show that recombinant adenovirus can engineer isolated islets to express a positron-emission tomography (PET) reporter gene and that these islets can be repeatedly imaged by using microPET after transplantation into mice. The magnitude of signal from engineered islets implanted into the axillary cavity was directly related to the implanted islet mass. PET signals attenuated over the following weeks because of the transient nature of adenovirus-mediated gene expression. Because the liver is the preferred site for islet implantation in humans, we also tested whether islets could be imaged after transfusion into the mouse liver. Control studies revealed that both intrahepatic islet transplantation and hyperglycemia altered the biodistribution kinetics of the PET probe systemically. Although transplanted islets were dispersed throughout the liver, clear signals from the liver region of mice receiving PET reporter-expressing islets were detectable for several weeks. Viral transduction, PET reporter expression, and repeated microPET imaging had no apparent deleterious effects on islet function after implantation. These studies lay a foundation for noninvasive quantitative assessments of islet graft survival using PET.

diabetes | transplantation

Type I diabetes (T1D) affects ≈1 in 300 individuals in the United States (1). Insulin administration does not fully restore glucose homeostasis, leading to long-term complications. When successful, islet transplantation can provide excellent metabolic control. However, most islet recipients gradually lose graft function. Because islets can up-regulate their production of insulin in response to need, measurements of blood glucose such as C peptide levels and first-phase insulin release only provide markers of the late stages of graft rejection (1). A noninvasive method of imaging islet grafts could allow the tailoring of immunosuppressive therapy to more effectively support islet survival after transplantation.

We, as well as others, recently showed that islets that had been engineered to express firefly luciferase could be monitored long-term after their transplantation in mice by using a cooled charge-coupled device (CCD) (2–4). However, bioluminescence imaging is currently limited to tissues not deeper than ≈2 cm (5). Positron-emission tomography (PET) imaging is used clinically to assess various disorders of the heart and brain and to detect various cancers (5, 6). In these applications, a positron-labeled PET probe is injected intravenously, binding to a target protein of interest, or is enzymatically converted to a "trapped" metabolic product, which can be detected tomographically and quantitatively imaged (6, 7). PET has been extended to small animals through the development of microPET technology (8, 9). Moreover, PET reporter gene systems have been developed that permit the noninvasive, quantitative, and repetitive assessment of reporter gene expression in small animal models (5, 10).

To image islets, the PET probes of choice would include substrates, ligands, or antibodies that are selectively taken up by or that bind to islet cells to a greater degree than their surrounding tissue. Although the development of islet-targeting probes is an active area of investigation, no satisfactory probes are currently available. We therefore sought to engineer isolated islets to express a PET reporter protein for which highly specific PET probes were available. This strategy parallels that of engineering cells and tissues to express luciferase and their subsequent imaging *in vivo* by using CCD.

Unlike luciferase substrates that are only converted to a bioluminescent form in cells that express luciferase, the probes used for PET imaging are radioactive and contribute background signals until they are cleared from tissues. Accordingly, the signal-to-noise ratio is usually much lower in PET than in optical imaging. When clinical PET scanners are used to image heart, brain, or tumors in humans, the signal from the target tissue is typically only 1.5- to 10-fold above background levels. Within this signal–background range, PET has high precision for detecting small differences in signal from a tissue in test–retest studies. For example, PET can be used to monitor the loss of dopaminergic neurons in Parkinson's disease even though dopaminergic neurons comprise only a small percent of the cells in the striatum and the PET signal from the striatum is typically ≈3-fold over background levels in healthy individuals (11). Thus, it is possible to use PET to longitudinally monitor the survival of a cell type that comprises only a small portion of an organ.

Here, we show that islets expressing a PET reporter gene can be longitudinally imaged using microPET after implantation into the mouse axillary cavity or liver. We discuss the challenges encountered in PET imaging of islet grafts in small animals and the potential for extending these technologies to humans.

Results and Discussion

Recombinant Adenovirus Directs the Expression of *sr39tk* in Transduced Islets. Thymidine kinase (TK) converts thymidine to thymidine monophosphate, which is trapped within cells. Herpes simplex virus (HSV) encodes its own TK (termed *HSV1-TK* and HSV1-tk for the gene and protein product, respectively), which

Conflict of interest statement: No conflicts declared.

Abbreviations: T1D, type 1 diabetes; CCD, cooled charge-coupled device; PET, positron-emission tomography; TK, thymidine kinase; HSV, herpes simplex virus; FHBG, 9-[4-fluoro-3-(hydroxymethyl)butyl]guanine; IEQ, islet equivalent; MOI, multiplicity of infection; NOD/SCID, nonobese diabetic/severe combined immunodeficient; STZ, streptozotocin; ROI, region of interest; %ID/g, percentage injected dose per gram of tissue.

‡To whom correspondence may be addressed. E-mail: mphelps@mednet.ucla.edu or dkaufman@mednet.ucla.edu.

© 2006 by The National Academy of Sciences of the USA

www.pnas.org/cgi/doi/10.1073/pnas.0603909103

Downloaded at Palestinian Territory, occupied on November 26, 2021

www.manaraa.com

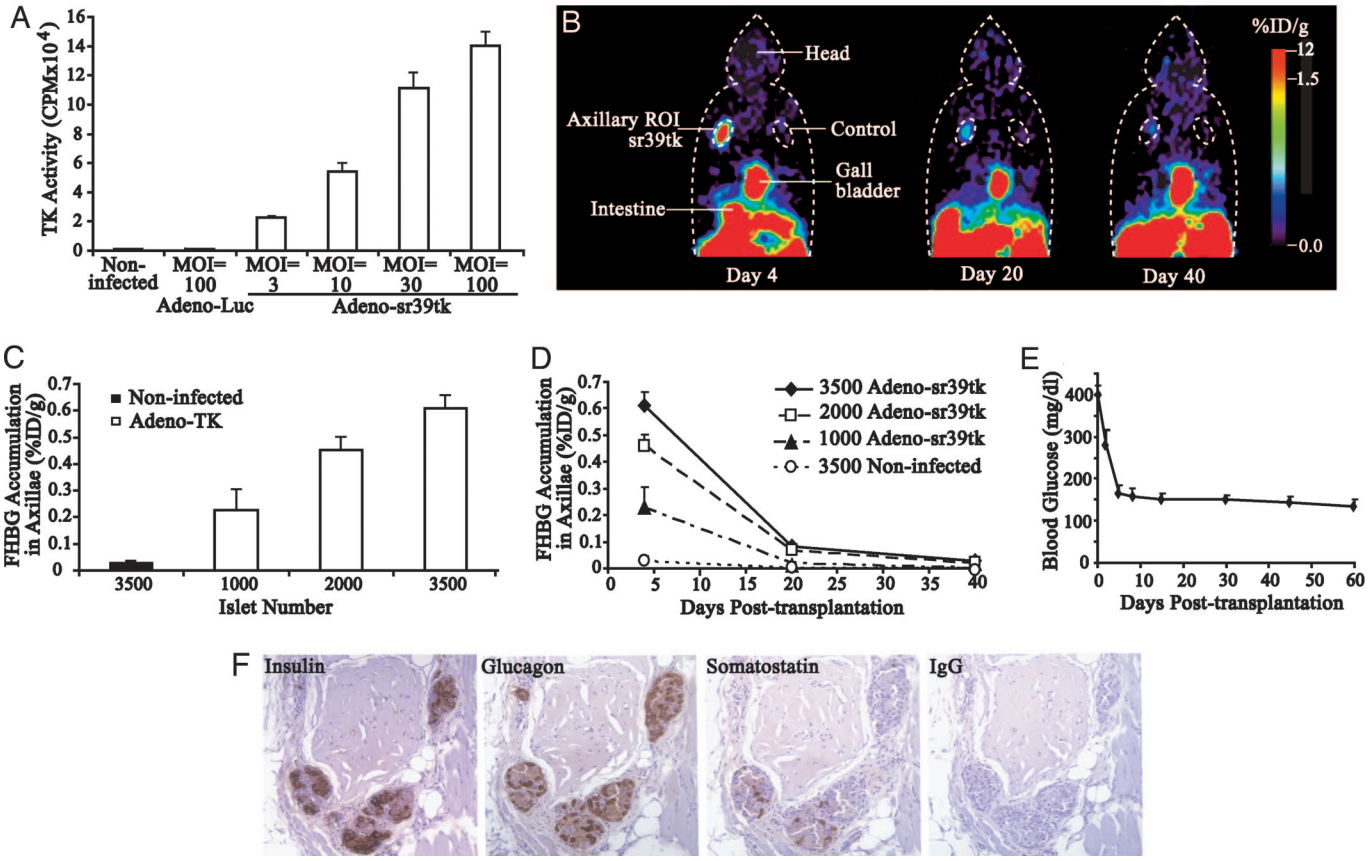

Fig. 1. MicroPET imaging islets implanted into the axillary cavity. (*A*) TK enzymatic activity in Adeno-sr39tk-infected human islets depends on the viral MOI. Human islets were or were not infected with Adeno-sr39tk (or control Adeno-Luc) at the indicated MOI. (*B*). Representative longitudinal microPET images of sr39tk-expressing human islets in the axillary cavity of an individual STZ-treated NOD/SCID mouse. The mouse shown was implanted with 3,500 IEQs that were uninfected (right shoulder, as a control) and transduced with Adeno-sr39tk (left shoulder). (*C*) MicroPET signal depends on the number of implanted engineered islets. Human islets (1,000, 2,000, or 3,500 IEQs) were infected with Adeno-sr39tk (MOI of 30), implanted into axillary cavities of NOD/SCID mice, and microPET-imaged 4 days later (open bars). A control group received 3,500 uninfected islets (filled bar). (*D*) Group data of longitudinal microPET signals from NOD/SCID mice implanted with 1,000, 2,000, or 3,500 sr39tk-expressing human islets or 3,500 uninfected islets. Data shown are the mean %ID/g signal from axilla minus background signal from chest ± SEM for each group. (*E*) Mean nonfasting glucose levels ± SEM of the mice receiving 3,500 sr39tk-expressing islets shown in *D*. (*F*) Sixty days after implantation (and 20 days after microPET signals returned to background levels), serial sections from axillary regions were immunostained for insulin, glucagon, somatostatin, or control rabbit IgG. There were no distinguishable differences with similarly stained uninfected islets (data not shown).

is necessary for its replication. Several drugs that have high affinity and specificity for HSV1-tk, compared with mammalian TK, are widely used against HSV infections. These substrates, such as 9-[4-fluoro-3-(hydroxymethyl)butyl]guanine (FHBG), can be positron-labeled so that cells engineered to express *HSV1-TK* can be imaged by PET (12). We used a mutant HSV1-tk gene, termed *HSV1-sr39tk*, that metabolizes FHBG more effectively (13). We chose a CMV promoter, rather than a β-cell-specific promoter (e.g., an insulin promoter), to drive the expression of sr39tk in islet cells because an insulin promoter would be regulated by blood glucose levels, confounding attempts to correlate PET signal with islet mass. Moreover, the major impediment to islet graft survival in humans is allograft rejection, which can be monitored by imaging islet cells *en masse*.

We began by optimizing the parameters for adenovirus-mediated sr39tk expression in cultured islets. Human islets [150 islet equivalents (IEQs)] were infected *in vitro* with Adeno-sr39tk at multiplicities of infection (MOIs) of 3, 10, 30, or 100. The same number of uninfected or Adeno-Luc-infected islets (MOI of 100) served as controls. The TK activity in homogenates of uninfected or Adeno-Luc-infected islets was at background levels (Fig. 1*A*). The magnitude of TK activity in Adeno-sr39tk-infected islet homogenates showed a dependence on the MOI. Islets infected with Adeno-sr39tk at MOIs of 30 and 100 had TK enzymatic activities that were ≈200- and 300-fold, respectively, over that of control islets. These data show that recombinant adenovirus can direct the expression of sr39tk in islets and that an MOI of 30 would be suitable in subsequent experiments.

MicroPET Imaging of Islets After Implantation into the Axillary Cavity. ^{18}F has a half-life of 109 min, necessitating that PET scanning occur soon after probe administration. Yet, sufficient time must be allowed for probe to accumulate in the target cells of interest while being eliminated from surrounding tissue. Because untrapped PET probe is eliminated through the gut and kidney, it can create spillover background signals in the pancreas, kidney, and liver regions of small animals until it is excreted. This spillover is not a problem in larger animals, because these organs are further apart and can be better tomographically resolved. To avoid background signals in our mice, we initially tested whether sr39tk-expressing islets could be imaged after implantation into the axillary cavity, which is far from the probe elimination pathway. Additionally, the implanted islets were confined to a relatively small volume, which should lead to a higher PET signal/volume, increasing our chances of detecting signals emanating from the islets.

Human islets (2,500 IEQs) were or were not transduced with Adeno-sr39tk and implanted into the axillary cavity of nonobese

Downloaded at Palestinian Territory, occupied on November 26, 2021
www.manaraa.com

diabetic/severe combined immunodeficient (NOD/SCID) mice. Four days later, the mice were microPET-imaged by using [^{18}F]FHBG as a probe. Based on previous imaging studies that used [^{18}F]FHBG (14), data were acquired between 60 and 75 min after probe injection. High signals were detected from the axillary region of mice that received Adeno-sr39tk transduced islets, whereas signals from uninfected islets were at background levels (a representative image is shown in Fig. 1*B*).

In a few cases, mice were imaged a few hours after they were implanted with control or sr39tk-expressing islets. Although signals from control islets were at background levels, the microPET signals from sr39tk-expressing islets were stronger than when the same mice were reimaged 6–12 days later (data not shown). Apparently, [^{18}F]FHBG has excellent accessibility to islets in the axillary cavity immediately after islet implantation, and islet vascularization is not a prerequisite for probe uptake/clearance and islet detection by PET.

The MicroPET Signal Is Directly Related to the Implanted Islet Mass. Human islets were transduced with Adeno-sr39tk, and 1,000, 2,000, or 3,500 islets were implanted into the axillary cavity of a NOD/SCID mouse. The mice that received 3,500 islets had been rendered diabetic by streptozotocin (STZ) treatment, and within a few days of transplantation these mice became euglycemic. Four days after transplantation, the mice were microPET-imaged by using [^{18}F]FHBG as a probe. The microPET signal from the axillary region of mice that received 3,500 uninfected islets was at background level (Fig. 1*C*). Axillary cavities implanted with 1,000, 2,000, and 3,500 sr39tk-expressing islets emitted signals ≈8-, 16-, and 22-fold greater, respectively, than that of 3,500 uninfected islets (Fig. 1*C*). There was a correlation between the number of implanted sr39tk-expressing islets and the magnitude of the microPET signal ($R^2 = 0.739$, $P = 0.03$).

Repeated MicroPET Imaging of Islets Transplanted into the Axillary Cavity. The islet recipients were repeatedly microPET-imaged over a 40-day period, during which the signals from the axillary regions implanted with sr39tk-expressing islets decreased to nearly background levels. This loss of signal was expected because of some islet cell death shortly after transplantation and the transient nature of adenovirus-directed gene expression. Representative longitudinal scans from a single mouse implanted with sr39tk-expressing islets are shown in Fig. 1*B*, and longitudinal group data are shown in Fig. 1*D*. Despite the loss of axillary signal by 40 days after transplantation, all of the islet recipients remained euglycemic throughout the 60-day observation period (Fig. 1*E*).

Twenty days after the microPET signals from the axilla reached background levels, some mice were killed, and the tissue containing the axillary cavity was histologically examined. When hematoxylin/eosin (H&E) staining was used, transplanted sr39tk-expressing islets had normal morphology with no inflammatory reaction. Immunohistochemical analysis showed apparently healthy islets expressing insulin, glucagon, and somatostatin (Fig. 1*F*).

Longitudinal MicroPET Imaging of Islets Implanted into the Mouse Liver. Because the liver is the preferred site of islet transplantation in humans, we next sought to image islets that were infused into the mouse liver. Imaging intrahepatic islets is technically challenging because the islets are dispersed over a large volume. Moreover, the liver is close to the probe excretion pathway, which can contribute background signals that may confound specific detection of liver signals.

Following previously described intrahepatic islet transplantation protocols (15, 16), we transfused 1,500–2,000 Adeno-Luc- or Adeno-sr39tk-infected rat islets into the mesenteric vein of STZ-treated diabetic NOD/SCID mice. Within a few days of implantation, the recipients' blood glucose levels returned to normal. Two to six days after implantation, the mice were microPET-imaged from 100 to 180 min after injection of [^{18}F]FHBG. Analysis of signal and signal-to-background ratios over time in liver regions of interest (ROIs) of mice that received sr39tk- vs. luciferase-expressing islets showed that a data acquisition time of 120–140 min after [^{18}F]FHBG injection was optimal for detecting signals from sr39tk-expressing islets. We also found that administration of sincalide (which causes the gallbladder to contract and expel its contents) just before data acquisition reduced signals from the gallbladder, allowing data collection from a larger area of the liver ROI. Representative microPET and CCD images of mice with intrahepatic sr39tk- and luciferase-expressing islets taken 4 days after transplantation are shown in Fig. 2*A*.

We then longitudinally monitored groups of diabetic STZ-treated NOD/SCID mice that received 1,500–2,000 uninfected, Adeno-sr39tk-infected, or Adeno-Luc-infected rat islets in their liver. We also scanned a control group of NOD/SCID mice that did not receive STZ or islets. The islet grafts reversed hyperglycemia in all STZ-treated mice within a few days. Although imaging analysis of axillary islet implants did not find any background differences in probe retention in mice that did or did not receive implants, we observed that, for the first several weeks after transplantation, recipients of uninfected or infected islets had higher background levels of probe in their chest and head regions compared with mice that did not receive implants (120–140 min after probe injection) (Fig. 2*B*). For example, 5 days after implantation, the background signals from the chest and head ROIs were ≈3-fold higher in mice that received intrahepatic islets than in mice that did not receive implants. The systemic retention of probe was much reduced when the mice were reimaged 20 days after implantation, and by 40 days after transplantation, there were no discernible systemic differences in probe retention between implanted and nonimplanted mice (Fig. 2*B*).

To better understand the basis for the systemic retention of probe after intrahepatic islet implantation, we further examined the effects of adenovirus infection, STZ treatment, intrahepatic islet implantation, and hyperglycemia on probe clearance kinetics 2–6 days after implantation (Fig. 2 *C* and *D*). We observed elevated chest and head background levels in STZ-treated NOD/SCID mice that received Adeno-sr39tk-infected or uninfected rat islets. The background levels in "normal" mice (without STZ treatment) implanted with uninfected islets were reduced, but this reduction did not quite reach statistical significance in this small study ($P = 0.07$). The background levels in normal mice implanted with uninfected islets were significantly higher those that in control mice that did not receive STZ or islets ($P = 0.02$) (Fig. 2*C*). These data suggest that (*i*) viral infection of islets does not affect probe retention, (*ii*) STZ treatment and/or transient hyperglycemia may contribute to the elevated background levels, and (*iii*) intrahepatic islet implantation is a major factor affecting probe clearance kinetics. We suspect that implantation-induced intrahepatic injuries initially affected portal blood flow and systemic probe clearance until compensatory mechanisms (e.g., angiogenesis and hepatocyte regeneration/remodeling) returned the biodistribution kinetics of [^{18}F]FHBG to normal conditions.

To examine the effects of hyperglycemia on probe clearance without the possible toxic side effects of STZ treatment, we microPET-imaged unmanipulated female NOD mice before and after they spontaneously developed T1D. Prediabetic mice were imaged at 16 weeks of age. After developing T1D, they were given insulin daily (3 units of Lantus; Sanofi-Aventis, Paris) and were reimaged at an average of 4 weeks after T1D onset. We observed significantly higher systemic probe background levels after they developed diabetes ($P = 0.005$) (Fig. 2*D*). Hence, the

Downloaded at Palestinian Territory, occupied on November 26, 2021

www.manaraa.com

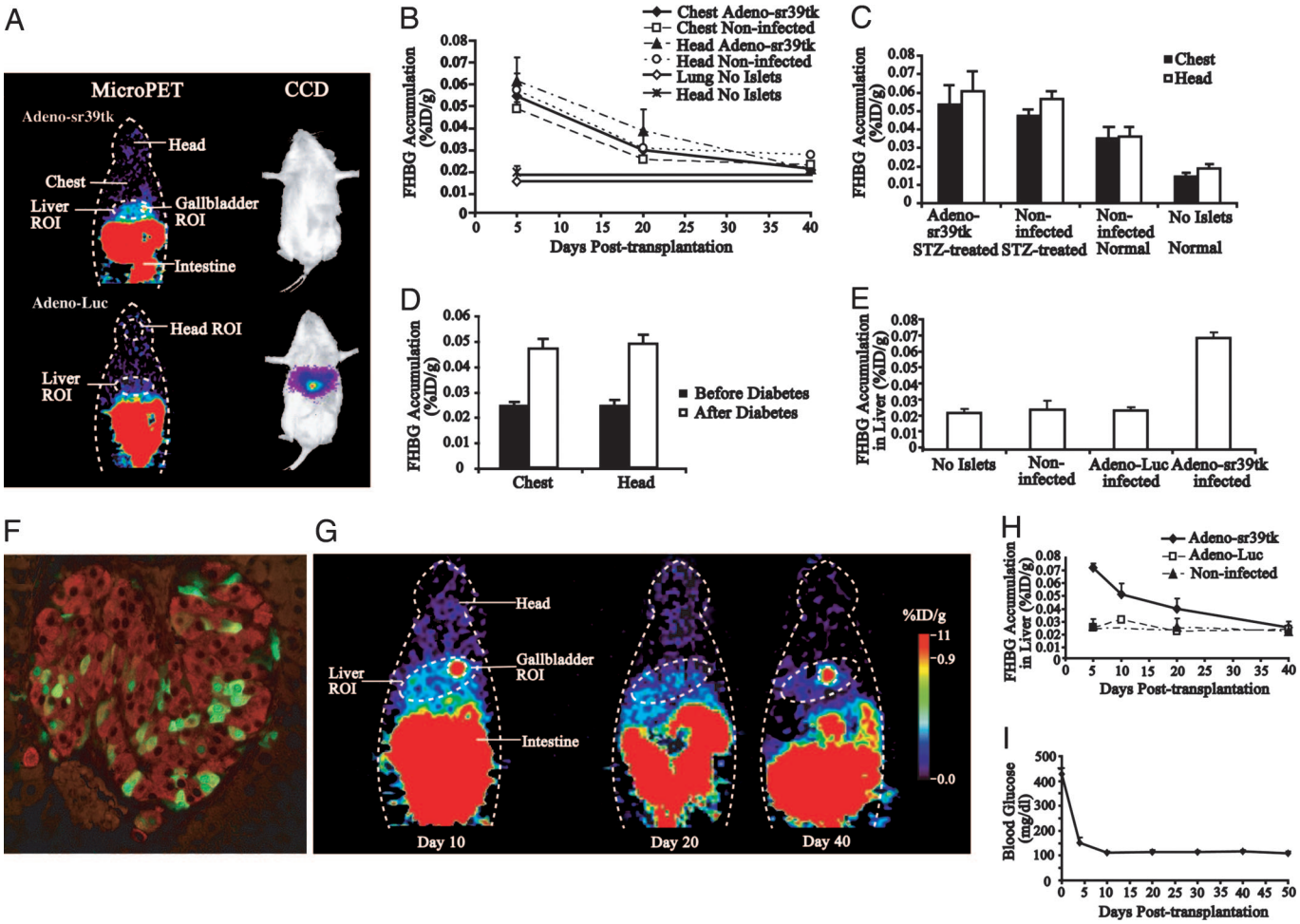

Fig. 2. MicroPET imaging islets implanted into the liver. (*A*) Representative coronal microPET images of mice implanted with Adeno-sr39tk-infected (*Left Upper*) or Adeno-Luc-infected (*Left Lower*) rat islets. Mice were imaged 4 days after transplantation, and data shown were acquired 120–140 min after [^{18}F]FHBG injection. The next day, the same mice were injected with D-Luciferin and CCD-imaged (*Right*) as described (2). (*B*) Background signals from the chest and head regions of mice that received adenovirus-infected or uninfected islets or no STZ or islets. Data shown are the mean %ID/g signal from chest or head regions ± SEM. (*C*) MicroPET signals from the chest and head region of STZ-treated or untreated (''normal'') NOD/SCID mice 2–6 days after receiving uninfected or Adeno-sr39tk-infected rat islets in their liver. A control group did not receive STZ or islets. (*D*) MicroPET signals from the chest and head region of NOD mice before and after spontaneously developing T1D. (*E*) Group data of microPET signals from the liver region of mice 2–6 days after receiving uninfected, Adeno-Luc-infected, or Adeno-sr39tk-infected islets in their liver. Another mouse group did not receive implants. Data shown are the mean liver %ID/g signal ± SEM of mice per group. The signal from livers with sr39tk-expressing islets was significantly greater than that from livers of the other control groups ($P = 0.0003$). (*F*) Histological analysis of sr39tk-expressing islets in the liver, 15 days after implantation. Coexpression of TK (green) with insulin (red) was observed in many scattered islet cells. (*G*) Longitudinal microPET imaging of a mouse with an intrahepatic islet graft. (*H*) Group data of longitudinal microPET signals from sr39tk-expressing islets, luciferase-expressing islets, or uninfected islets implanted into the liver of STZ-treated NOD/SCID mice. (*I*) Mean nonfasting glucose levels ± SEM of the mice receiving sr39tk-expressing islets shown in *E*.

metabolic imbalances that accompany T1D cause changes in the systemic distribution or retention of the nucleoside [^{18}F]FHBG. Transient hyperglycemia may have contributed to the higher backgrounds in the STZ-treated mice that received intrahepatic islets (Fig. 2*C*). Together, these observations indicate that intrahepatic islet transplantation and hyperglycemia can significantly alter the biodistribution kinetics of PET probe systemically.

Because of the initially higher probe background levels in islet recipients, it was useful to subtract the background (measured by using a chest ROI) from the signals obtained from the liver ROI. We also excluded the signals from the gallbladder, which was inside of the liver ROI. By using these parameters, 4 days after transplantation, the signals from the liver region of a group of mice implanted with sr39tk-expressing islets were ≈3-fold above those of groups of mice implanted with luciferase-expressing islets or uninfected islets or signals from the liver region of mice without implanted islets (Fig. 2*E*) ($P < 0.002$ for Adeno-sr39tk vs. any of the control groups).

When the mice were reimaged 10 days after transplantation, signals from the liver area of sr39tk-expressing islets were ≈2-fold higher than in mice that received luciferase-expressing islets or that did not receive islet grafts. Immunohistological analysis of livers 15 days after implanting sr39tk-expressing islets showed healthy islets were dispersed throughout all liver lobes and expressed both insulin and TK (Fig. 2*F*) Representative longitudinal images of an individual mouse are shown in Fig. 2*G*, and longitudinal group data are shown in Fig. 2*H*. The signals from sr39tk-expressing islets continued to decline with time, such that, at 20 days after transplantation, signals from the liver region of sr39tk-expressing islets were ≈1.5-fold over levels in mice that received control islets. When imaged 40 days after transplantation, signals from the liver area were essentially at background levels. The loss of signal from sr39tk-expressing islets was likely due to some cellular death shortly after implantation and the transient nature of adenovirus-directed gene

Downloaded at Palestinian Territory, occupied on November 26, 2021
www.manaraa.com

expression. The mice remained euglycemic throughout the 50-day observation period (Fig. 2*I*). Livers examined 50 days after implantation had healthy insulin-expressing islets (data not shown).

The signal from intrahepatic islets was weaker than that from a similar number of islets in the axillary cavity, as was expected because the islets were dispersed in a larger volume in the liver. However, it is difficult to compare the signals from islets implanted into the axillary cavity and liver because (*i*) the islets came from different species, (*ii*) the islets may have different islet survival rates in the two transplantation sites, and (*iii*) the two sites were imaged at different time points after probe injection. The important point is that signals from liver regions with implanted islets were severalfold higher than the background. This signal-to-background ratio is similar to that obtained in various clinical PET applications. Therefore, PET imaging is a promising technology for detecting loss of islet mass before abnormalities in islet function are detected in the blood.

Conceivably, isolated islets may be engineered to express immunomodulatory genes that will prolong their survival after implantation. If the immunomodulatory gene is transcriptionally linked with a PET reporter gene, it could allow clinicians to indirectly monitor both the expression levels of the immunotherapeutic gene and islet graft survival (10). Notably, we recently PET-imaged gene delivery in cancer patients using FHBG, setting an example of our approach in a clinical situation (17).

Because of the small size of mice, we had to wait for probe to clear from the gut/kidney to avoid spillover signals into the liver ROI. In larger animals and humans, the liver area can be readily distinguished tomographically from gut/kidney. Background signals from the probe excretion pathway could also be reduced by using PET probes with longer half-lives [e.g., ^{124}I-1-(2′-deoxy-2′-fluoro-β-D-arabinofuranosoyl)-5-iodouracil (^{124}I-FIAU) has a half-life of 48 h] and waiting for the probe to be excreted before imaging (18).

Nonengineered islets may be PET-imaged once islet-reactive antibodies, or ligands/substrates, that bind or are sequestered by islet cells to a greater degree than surrounding tissues become available. PET probe and PET scanner technologies are constantly evolving to enhance sensitivity and resolution (19). The combination of new islet-specific probes and imaging technologies may provide powerful new tools to monitor and prolong the survival of islets in individuals at risk for, or with, type 1 or 2 diabetes.

Materials and Methods

Recombinant Adenovirus Vectors. Recombinant adenoviruses that express sr39tk or firefly luciferase (Luc) under the control of a CMV promoter (Adeno-sr39tk and Adeno-Luc, respectively) have been described (13, 20).

Transduction of Human and Rodent Islets. Human islets (≥80% purity) provided by the network of Juvenile Diabetes Research Foundation International (JDRF) Human Islet Distribution Programmes (Washington, DC) or the National Institutes of Health (NIH) Islet Distribution Program (Bethesda) were used in *in vitro* assays of TK activity and in imaging studies of islet grafts in the mouse axillary cavity. Because of the limited availability of human islets, rat islets (Sprague–Dawley rats from Taconic Farms) were used in liver implantation studies. Rat islets were isolated by mechanical and enzymatic digestion of pancreata followed by gradient centrifugation. The human or rat islets were cultured in CMRL medium (Invitrogen), 10% FCS (HyClone), L-glutamine (2 mM), and antibiotics. The islets were infected with recombinant adenovirus at the indicated MOI for 1 h at 37°C, followed by medium addition and overnight culture. MOI calculations were based on the generalization that a human or rat islet contains an average of 2,000 cells (21). The islets were collected and washed three times with PBS, and the indicated numbers of untransduced and transduced islets were tested in *in vitro* assays or implanted into a mouse axillary cavity or liver.

TK Enzyme Assay. A total of 150 human IEQs were infected (in triplicate) as described above, incubated for 48 h, and homogenized. TK enzymatic activity in lysates was measured as described elsewhere (13, 22). Results are reported as the mean cpm/0.2 μg of protein/min ± SEM (n = 4 wells per group).

Mice. Eight- to 12-week-old male NOD/SCID mice (Taconic Farms) served as islet recipients. Some NOD/SCID mice were rendered diabetic before receiving islets by STZ treatment (100 mg/kg i.p., followed by 60 mg/kg the next day). Mice were considered diabetic when their nonfasting blood glucose levels were >300 mg/dl on 2 consecutive days. The University of California, Los Angeles (UCLA) Animal Research committee approved all animal care and experimental procedures.

Islet Implantation into Axillary Cavities. Human islets were or were not infected with recombinant adenovirus as detailed above. The indicated numbers of islets were washed three times with sterile PBS, and the last pellet was mixed with 20 μl of matrigel (BD Biosciences, Franklin Lakes, NJ) in a final volume of 40–60 μl and implanted into an axillary cavity of an untreated or an STZ-treated diabetic NOD/SCID mouse. Blood glucose values were monitored daily until euglycemia was restored and then twice weekly thereafter. The islet recipients were microPET-imaged at the indicated time points.

Islet Implantation into the Mouse Liver. As in previous studies (15, 16), we implanted 1,500–2,000 rat islets into a mouse liver. Briefly, rat islets (infected or uninfected) were washed three times and suspended in 200 μl of PBS. The islets were slowly (over ≈40 s) intraportally injected via a mesenteric vein of a NOD/SCID mouse. Gelform (Amersham Pharmacia) was applied to the injection site and the incision was bilayerly sutured. The recipient's nonfasting blood glucose was monitored daily until euglycemia was restored and then twice weekly thereafter. The mice were microPET-imaged at the indicated time points.

MicroPET Imaging. Mice were imaged by using the microPET Focus system (CTI Concorde Microsystems, Knoxville, TN) (9). Mice were injected via tail vein with 200- or 250-μCi (1 Ci = 37 GBq) PET reporter probe [^{18}F]FHBG [specific activity of 5–10 Ci/mmol (22)], for imaging axillary and liver implants, respectively. For axillary imaging, anesthetized mice were imaged 60–75 min after probe injection. For liver imaging, time course studies (100–180 min after probe injection) indicated that intrahepatic islets were optimally imaged 120–140 min after probe injection. Before liver imaging, sincalide (Bracco Diagnostics, Princeton) was given twice through the tail vein (0.06 μg/kg in 100 μl of PBS) 15 min before and immediately before microPET scanning to expel probe from the gallbladder. Images were created by using a filtered back-projection reconstruction algorithm. The animals were reimaged at the indicated time points after transplantation. After islet signals reached background levels, some mice were killed, and the tissues were processed for immunocytochemistry. Some mice were also imaged by using a CCD, as described (2).

MicroPET Data Analysis. MicroPET data were analyzed by using AMIDE 0.8.7 software (http://amide.sourceforge.net). In axillary islet transplantation studies, the absolute maximum threshold was set to 1×10^4 PET units for image display. For each mouse, a 3D ROI was drawn around the axillary area to closely encompass the islet signal, which could be viewed simultaneously on the transverse, coronal, and sagittal images. The ROI pa-

Downloaded at Palestinian Territory, occupied on November 26, 2021
www.manaraa.com

rameters from the first PET imaging were saved for signal measurement on the same mouse at later time points. PET units from the ROIs were converted to counts per ml/min by using a calibration constant obtained from imaging a mouse-size cylindrical phantom with a known activity concentration of ^{18}F. The ROI counts per ml/min were converted to counts per g/min (assuming a tissue density of 1 g/ml) and divided by injected dose to obtain an image ROI-derived [^{18}F]FHBG percentage injected dose per gram of tissue (%ID/g). The mean value of ROI signal reading was directly used as PET units for %ID/g calculation. The signal from the mouse's chest region (within a volume equal to that of the axillary ROI) provided a background measurement. The signal from the islet graft was corrected for background by subtracting the chest ROI signal. Group data were expressed as FHBG accumulation in axillae %ID/g ± SEM (n = 3 mice per group).

In liver islet transplantation studies, the absolute maximum threshold was raised to 3×10^5 PET units for image display to better discern liver signals from spillover signals from the gallbladder and intestine. A 3D ROI was drawn in the liver region, well above the intestines. This liver ROI ranged from 1.2–1.8 cm^3 in different mice. Another ROI was drawn to encompass the gallbladder (gallbladder ROI), which was within the liver ROI. To measure background levels, a ROI was drawn on the mouse's chest (chest ROI) that had a volume equal to the liver ROI minus the gallbladder ROI in that mouse. Data were also acquired from the head region (head ROI), which had a volume of 600 mm^3. The mean value of liver ROI was calculated as the total value of (liver ROI − gallbladder ROI − chest ROI) divided by the fractional voxel value of (liver ROI − gallbladder ROI). This mean value was then used to calculate the liver signal %ID/g. Group data were expressed as FHBG accumulation in liver %ID/g ± SEM (n = 3 mice per group). Group data were analyzed with a two-tailed Student's t test.

Histology. After repeated microPET imaging, some mice were killed at the indicated time point, the axillary region or the liver was removed, and sections were analyzed by immunohistochemistry as described (2, 23).

Note Added in Proof. Souza *et al.* (24) recently reported a probe for PET imaging β cells.

We thank the network of the Juvenile Diabetes Research Foundation International (JDRF) Human Islet Distribution Programmes and the National Institutes of Health (NIH) National Islet Cell Resource Center Program, particularly the centers at the University of Miami (Coral Gables, FL), University of Minnesota (Minneapolis), Washington University (St. Louis), and the City of Hope (Duarte, CA), as well as Dr. David Harlan (National Institute of Diabetes and Digestive and Kidney Diseases, NIH) for human islets. We also thank members of the Crump Institute for Molecular Imaging, University of California, Los Angeles (UCLA) for advice and technical expertise and Drs. Harvey Herschman and Lily Wu (UCLA) for providing Adeno-sr39tk. This work was supported by NIH grants R01 DK58514, R01 DK068506, R21 DK069839 (to D.L.K.), and R01 CA82214-01 (to S.S.G.); Department of Energy contracts DE-FC03-87ER60615 (to S.S.G.) and DE-FC03-02ER63420 (to D.L.K.); National Cancer Institute Small Animal Imaging Resource Program Grant R24 CA92865 (to S.S.G.); and the JDRF (D.L.K., M.A.A., and M.C.-T.).

1. Atkinson, M. A. & Maclaren, N. K. (1994) *N. Engl. J. Med.* **331,** 1428–1436.
2. Lu, Y., Dang, H., Middleton, B., Zhang, Z., Washburn, L., Campbell-Thompson, M., Atkinson, M. A., Gambhir, S. S., Tian, J. & Kaufman, D. L. (2004) *Mol. Ther.* **9,** 428–435.
3. Fowler, M., Virostko, J., Chen, Z., Poffenberger, G., Radhika, A., Brissova, M., Shiota, M., Nicholson, W. E., Shi, Y., Hirshberg, B., *et al.* (2005) *Transplantation* **79,** 768–776.
4. Park, S. Y., Wang, X., Chen, Z., Powers, A. C., Magnuson, M. A., Head, W. S., Piston, D. W. & Bell, G. I. (2005) *Genesis* **43,** 80–86.
5. Massoud, T. F. & Gambhir, S. S. (2003) *Genes Dev.* **17,** 545–580.
6. Phelps, M. E. (2000) *Proc. Natl. Acad. Sci. USA* **97,** 9226–9233.
7. Gambhir, S. S. (2004) in *PET: Molecular Imaging and Its Biological Applications*, ed. Phelps, M. E. (Springer, New York), pp. 125–216.
8. Chatziioannou, A. F., Cherry, S. R., Shao, Y., Silverman, R. W., Meadors, K., Farquhar, T. H., Pedarsani, M. & Phelps, M. E. (1999) *J. Nucl. Med.* **40,** 1164–1175.
9. Tai, C., Chatziioannou, A., Siegel, S., Young, J., Newport, D., Goble, R. N., Nutt, R. E. & Cherry, S. R. (2001) *Phys. Med. Biol.* **46,** 1845–1862.
10. Yu, Y., Annala, A. J., Barrio, J. R., Toyokuni, T., Satyamurthy, N., Namavari, M., Cherry, S. R., Phelps, M. E., Herschman, H. R. & Gambhir, S. S. (2000) *Nat. Med.* **6,** 933–937.
11. Morrish, P. K., Sawle, G. V. & Brooks, D. J. (1996) *Brain* **119,** 585–591.
12. Alauddin, M. M. & Conti, P. S. (1998) *Nucl. Med. Biol.* **25,** 175–180.
13. Gambhir, S. S., Bauer, E., Black, M. E., Liang, Q., Kokoris, M. S., Barrio, J. R., Iyer, M., Namavari, M., Phelps, M. E. & Herschman, H. R. (2000) *Proc. Natl. Acad. Sci. USA* **97,** 2785–2790.
14. Gambhir, S. S., Barrio, J. R., Phelps, M. E., Iyer, M., Namavari, M., Satyamurthy, N., Wu, L., Green, L. A., Bauer, E., MacLaren, D. C., *et al.* (1999) *Proc. Natl. Acad. Sci. USA* **96,** 2333–2338.
15. Okitsu, T., Bartlett, S. T., Hadley, G. A., Drachenberg, C. B. & Farney, A. C. (2001) *Am. J. Transplant.* **1,** 138–145.
16. Hara, M., Yin, D., Dizon, R. F., Shen, J., Chong, A. S. & Bindokas, V. P. (2004) *Transplantation* **78,** 615–618.
17. Penuelas, I., Mazzollini, G., Boan, J. F., Sangro, B., Marti-Climent, J., Ruiz, M., Ruiz, J., Satyamurthy, N., Qian, C., Barrio, J. R., *et al.* (2005) *Gastroenterology* **128,** 1787–1795.
18. Kang, K. W., Min, J. J., Chen, X. & Gambhir, S. S. (2006) *Mol. Imaging Biol.*, in press.
19. Phelps, M. E., ed. (2004) *PET: Molecular Imaging and Its Biological Applications* (Springer, New York).
20. Wu, J. C., Sundaresan, G., Iyer, M. & Gambhir, S. S. (2001) *Mol. Ther.* **4,** 297–306.
21. Bonner-Weir, S. (1991) in *The Endocrine Pancreas: Anatomy of the Islet of Langerhans*, ed. Samols, Ellis (Raven, New York), pp. 15–27.
22. Yaghoubi, S., Barrio, J. R., Dahlbom, M., Iyer, M., Namavari, M., Satyamurthy, N., Goldman, R., Herschman, H. R., Phelps, M. E. & Gambhir, S. S. (2001) *J. Nucl. Med.* **42,** 1225–1234.
23. Zhang, Y. C., Pileggi, A., Agarwal, A., Molano, R. D., Powers, M., Brusko, T., Wasserfall, C., Goudy, K., Zahr, E., Poggioli, R., *et al.* (2003) *Diabetes* **52,** 708–716.
24 Souza, F., Simpson, N., Raffo, A., Saxena, C., Maffei, A., Hardy, M., Kilbourn, M., Goland, R., Leibel, R., Mann, J. J., *et al.* (2006) *J. Clin. Invest.* **116,** 1506–1513.

Downloaded at Palestinian Territory, occupied on November 26, 2021

www.manaraa.com